

FAST-IDS: A Fast Two-Stage Intrusion Detection System with Hybrid Compression for Real-Time Threat Detection in Connected and Autonomous Vehicles

Devika S, Vishnu Hari, Pratik Narang, *Senior Member, IEEE*, Tejasvi Alladi, *Senior Member, IEEE*, and Vinay Chamola, *Senior Member, IEEE*

Abstract—In the realm of Intelligent Transportation Systems (ITS) and Connected and Autonomous Vehicles (CAVs), the ever-growing connectivity among vehicles, roadside infrastructure, and the Internet opens the door to a wide array of cybersecurity threats. Intrusion Detection Systems (IDSs) have thus been essential for ensuring safety and efficiency in ITS. While prior studies highlight the importance of detecting novel attacks, adopting multi-stage IDS architectures, and maintaining computational efficiency, only a few frameworks address all these aspects collectively, and many overlook deployment in resource-constrained environments. To address these gaps, we introduce a novel two-stage IDS optimized through hybrid model compression, integrating structural pruning and static quantization, achieving a 77.2% reduction in model size while maintaining computational efficiency. Validated on the VeReMi Extension dataset, the lightweight model supports real-time deployment on RTX A6000, Colab CPU, and Jetson Nano, achieving per-vehicle attack detection within 0.195 seconds, achieving approximately 50.05% reduction in inference time. The first stage employs a coarse-grained 4-layer Convolutional Neural Network (CNN) integrated with a Bidirectional Generative Adversarial Network (BiGAN) to identify normal versus anomalous vehicular data, achieving a recall rate of 92.79%. The second stage employs a fine-grained hybrid CNN-Long Short-Term Memory (CNN-LSTM) classifier, featuring a 2-layer CNN and a 1-layer LSTM, to discriminate among 19 known attack types with an accuracy rate of 97.822%. By leveraging reconstruction error metrics and combining supervised with unsupervised techniques, the proposed framework significantly enhances the detection of zero-day attacks. Experimental evaluations show that the proposed IDS surpasses existing methods, offering a robust and scalable cybersecurity solution for next-generation intelligent transportation.

Index Terms—Access Control, Cryptography, Bidirectional Generative Adversarial Networks (BiGANs), Connected and Autonomous Vehicles (CAVs), Convolutional Neural Network (CNN), Long Short Term Memory (LSTM), Intrusion detection

I. INTRODUCTION

Connected and Autonomous Vehicles (CAVs) are integrated networks that facilitate communication with other vehicles

Devika S, Vishnu Hari, Pratik Narang and Tejasvi Alladi are with the Department of Computer Science and Information Systems, BITS Pilani, Pilani Campus, 333031, India. (e-mail: p20210024@pilani.bits-pilani.ac.in; f20220094@pilani.bits-pilani.ac.in; pratik.narang@pilani.bits-pilani.ac.in; tejasvi.alladi@pilani.bits-pilani.ac.in).

Vinay Chamola is with the Department of Electrical and Electronics Engineering & APPCAIR, BITS Pilani, Pilani Campus, 333031, India. (e-mail: vinay.chamola@pilani.bits-pilani.ac.in).

within a specified range and exhibit varying levels of autonomy. The development of CAVs has been motivated by enhanced road safety, advancements in communication technology, economic benefits and user requirements, thereby achieving the objectives of Intelligent Transport Systems (ITSs) [1, 2]. The full functionality of CAVs relies on continuous connectivity within a specified range, using the IEEE 802.11 standard for the allocated 5.9 GHz frequency band [3]. The IEEE 802.11 standard, which resembles Wi-Fi technology, enables vehicles to connect with other vehicles (Vehicle-to-Vehicle), roadside infrastructure (Vehicle-to-Infrastructure), cloud servers (Vehicle-to-Cloud), pedestrians (Vehicle-to-Pedestrian) and essentially everything else (Vehicle-to-Everything) [4].

According to the World Health Organization (2019), traffic accidents accounted for 93% of all fatalities, resulting in 1.3 million deaths. While CAVs can significantly reduce accidents caused by human error, their increasing connectivity through Basic Safety Messages (BSMs) exposes them to privacy risks and cyber threats. Consequently, robust solutions, including Blockchain technology [5], cryptography-based encryption [6], and authentication schemes [7, 8], have been developed to protect CAVs.

However, encryption techniques alone proved inefficient, introducing an Intrusion Detection System (IDS). IDS proved crucial to complement encryption-based security [9] by providing network-wide monitoring and protecting individual communication links in vehicular networks. The dynamic and heterogeneous nature of cyber threats necessitates a robust IDS framework [9], with deep learning models being well-suited due to the vast data exchange among vehicles. IDS have evolved significantly, progressing from plausibility checks [10] to advanced deep learning models [11, 12].

Recent studies implemented on hybrid deep learning models and generative AI models have effectively addressed challenges in IDS. For instance, [13] combined machine learning and deep learning models to improve intrusion detection on benchmarked datasets, though several of the datasets used were outdated. Whereas, [12] proposed an optimized CNN architecture targeting physical-layer message features. Additionally, multi-stage intrusion detection [9, 14–16] enhances performance compared to single-stage classifiers and also addresses computational latency, which is vital for efficient

operation in resource-constrained vehicular environments [17, 18]. Specifically, [19] demonstrated multi-stage detection with an ANN for Stage 1 and LSTM being utilized in Stage 2, demonstrating effectiveness against previously unseen attacks. Generative AI, particularly Generative Adversarial Networks (GANs), was proven effective in detecting anomalies through its reconstructive properties [11, 20], enabling the identification of unseen attacks [21]. However, despite these advantages, they fall short in comprehensively addressing zero-day attack detection, a lightweight model that can be deployed in a resource-constrained environment and achieving fast real-time response. Motivated by these challenges, we developed a two-stage IDS utilizing Bidirectional Generative Adversarial Network (BiGAN) [22] with Wasserstein loss and gradient penalty in Stage 1 and hybrid CNN-LSTM in Stage 2. Our two-stage model integrates model compression to minimize computational latency and thereby effective for deployment on resource-constrained platforms while ensuring high detection accuracy and fast inference.

The contributions of this study are:

- i. Two-Stage Intrusion Detection Framework: We utilized the capabilities of BiGAN for coarse-grained anomaly detection (Stage 1) and CNN-LSTM for fine-grained classification (Stage 2), resulting in a robust hybrid model that significantly enhances the security in CAVs.
- ii. Hybrid Model Compression: We proposed a model compression technique combining structural pruning with static quantization, achieving a 50.05% reduction in inference time and a 77.2% reduction in model size, with approximately 5% performance loss. The inference performance was evaluated on RTX A6000 GPU, Colab CPU, and Jetson Nano, with a per-vehicle detection time of 0.195 seconds in real time.
- iii. Detection of Previously Unseen Attacks: Stage 1 applied unsupervised metrics (MSE, Mahalanobis distance) for anomaly detection, while Stage 2 used supervised learning to refine detection and identify unseen attacks. This hybrid supervised-unsupervised approach improved performance, achieving 85.05% accuracy on unseen threats while maintaining strong detection of known attacks.
- iv. Performance Metrics Evaluation: We achieved a recall rate of 92.785% in the first stage for classifying data as normal or anomalous, and accuracy rate of 97.822% in the second stage for classifying anomalous data into 19 known attack types, surpassing existing state-of-the-art (SOTA) methods.

The rest of this paper is organized as follows: Section II surveys the related works. Section III provides a preliminary background, including the CAV scenario, the dataset used, and the taxonomy of attacks within the scope of this study. Section IV outlines the proposed intrusion detection architecture, detailing Stages 1 and 2, followed by the hybrid data compression implementation. Section V describes the experimental setup, while Section VI presents the results and analysis. Finally, Section VII concludes the study.

II. RELATED WORK

This section presents a comprehensive review of existing intrusion detection research in CAVs. Table I provides a detailed comparison, highlighting datasets used, attack coverage, multistage detection capability, zero-day attack identification, and computational latency considerations.

1) *Intrusion Detection Systems in CAVs*: The deployment of Hybrid CNN-LSTM models on Multi-access Edge Computing (MEC) servers for attack classification was explored in [2], utilizing LSTMs for sequence-based classification and CNNs for sequence-image classification, enabling real-time processing. The study in [23] introduced the Burwood SUMO Traffic (BurST) dataset, simulating Australian traffic conditions and employing supervised learning algorithms such as KNN, SVM, Naive Bayes, and Random Forest for attack classification. In [25], plausibility checks, including Location and Movement Plausibility, were integrated into supervised learning models for attack detection in CAVs. Authors in [28] segmented vehicular data [10] into frequency (timestamp), identity (pseudo-identity), and motion, processing them through three CNN-based reconstruction models with branching and reconstruction error thresholds.

2) *Computational Efficiency in Resource Constrained Environments*: The study in [17] addressed computational latency by compressing Controller Area Network (CAN) messages through XOR-based encoding, transmitting only the differences between consecutive frames while utilizing the dedicated Compression Area Map (CAP) to preserve data integrity. Similarly, [18] adopted a bitmap-based compression method for malicious traffic, incorporating a predefined threshold and a relearning step that reduced memory consumption and training time. While [28] proposed a CNN-based reconstruction approach for IDS, emphasizing deployment in resource-constrained environments such as Jetson Nano and Google Colab, with applicability to edge and cloud platforms. Another notable improvement is presented in [29], where the authors have performed feature selection, handling of missing data, and dimensionality reduction using a deep machine learning algorithm. Although this work is from the medical domain, it is highly relevant to our work and provides a valuable direction for the future. Though effective in computing, their optimizations are mainly restricted to the data level or struggle to achieve robust performance in real-world implementations.

3) *GANs for Intrusion Detection*: Authors in [11] propose an unsupervised GAN framework for attack detection in CAVs, leveraging reconstruction properties to detect previously unseen attacks while focusing on motion-related attributes from the VeReMi Extension dataset. The authors of [20] present a GAN-based intrusion detection method for automotive CAN networks, enhancing attack detection by integrating the CAN communication matrix to identify threats like DoS, injection, masquerade, and data tampering. The work in [21] introduces a multi-stage GAN-based IDS for CAN networks, incorporating an Auxiliary Classifier GAN (ACGAN) and Out-of-Distribution (OOD) detection to improve identification of both known and unknown attacks. While these reconstruction-based mechanisms claim the detection of previously unseen attacks, their detection capability remains uncertain.

TABLE I: Comparative Study

S. No.	Ref.	Dataset - Attacks	Models Used	Multistage Detection	Unseen Attacks	Is Computational Efficiency talked about ?
1	[2]	VeReMi Extension-19	Hybrid cnn-lstm	X	X	✓
2	[23]	BurST-ADMA-7	Supervised ML	X	X	X
3	[24]	VeReMi - 8	CNN + Self-attention	X	✓	✓
4	[25]	VeReMi - 5	Supervised ML, Ensemble	X	X	X
5	[26]	VeReMi - 5	DL	X	✓	X
6	[9]	VeReMi Extension-17	Hybrid cnn-lstm	✓	X	✓
7	[11]	VereMiExtension-19	GAN	X	✓	✓
8	[20]	CAN-10	GAN	X	✓	X
9	[27]	Car Hack2020 - 5	LSTM, GRU	X	X	X
10	[28]	VeReMi Extension-19	CNN + Reconstruction	X	✓	✓

4) *Detection of Unseen Attacks:* The research in [24] utilizes a CNN and a self-attention mechanism for feature extraction. Although the authors claim to detect new attacks over time using their update mechanism, they do not explicitly show any results. Similarly, the authors in [26] have demonstrated that models such as Logistic Regression and LSTM failed to detect adversarial perturbations and did not devise any IDS capable of detecting them. Implementing GANs [11, 20, 21] in intrusion detection enhances the detection of previously unseen attacks by training the generator to create adversarial examples and the discriminator to recognize new attack patterns. While they have achieved good performance in detecting known attacks, they have not shown the detection of previously unseen attacks.

5) *Multistage Intrusion Detection:* The work in [9] implements three Deep Learning Classifier Engines (DLCE-1, DLCE-2, DLCE-3) in single-stage and multi-stage configurations on edge servers, enhancing security and reducing computational latency using Hybrid CNN-LSTM models. A multi-stage intrusion detection system in [14] utilizes a Hidden Markov Model (HMM) to identify intrusions through characteristic signals while distributing workload to minimize overhead. The LSTM-based autoencoder proposed in [15] captures long-term dependencies for multi-stage attack detection across four public datasets, with a multi-encoder approach improving efficiency for real-time intrusion detection. However, the VeReMi extension dataset remains underutilized in multi-stage IDS, and effective integration of factors such as unseen attack detection and lightweight model deployment in resource-constrained environments is still lacking.

Our comprehensive literature review underscored the need for an IDS that integrates model compression to mitigate computational latency, generative AI to exploit reconstructive properties for detecting previously unseen attacks, and a multistage architecture to capture long-term dependencies in time-series data. These insights led to developing our two-stage intrusion detection model, providing a fast and efficient real-time solution.

III. PRELIMINARY BACKGROUND

1) *CAV Scenario:* Fig. 1 illustrates a typical CAV scenario where vehicles communicate via Vehicle-to-Vehicle (V2V) and Vehicle-to-Infrastructure (V2I) networks. Each vehicle

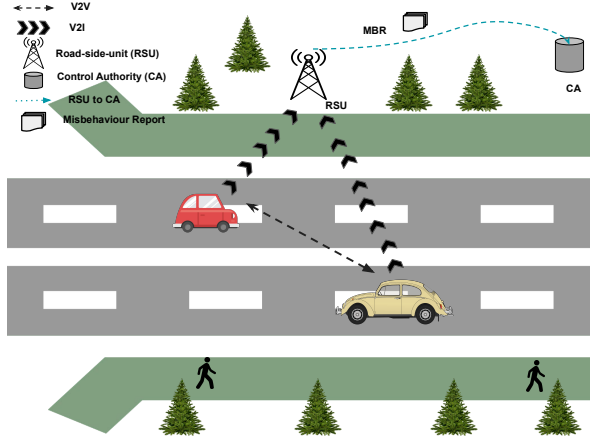


Fig. 1: A typical CAV scenario.

processes GPS and sensor data locally through an On-Board Unit (OBU). The vehicles must register with a Control Authority (CA) for authentication within its operational area [9]. Roadside Units (RSUs) manage message transmission and intrusion detection, analyzing received data to detect potential attacks. A Misbehaviour Report (MBR) is generated and sent to the CA if a message is flagged as anomalous. Based on the received MBRs, the CA can take appropriate actions, such as revoking the vehicle's certificate, to mitigate security threats if necessary.

2) *Dataset:* The VeReMi Extension dataset [10], an enhancement of the original VeReMi dataset [30], is used in our IDS evaluation. The dataset is generated using the Framework for Misbehaviour Detection (F2MD), an extension of VEINS, integrating OMNeT++ for network simulation and SUMO [31] for traffic simulation, and is validated using real-vehicular data from Luxembourg. Realistic sensor error models for position, speed, acceleration, and heading ensure accurate simulation based on real GPS and vehicular data. The dataset includes sender vehicle ID, timestamp, pseudo-identity, message ID, and vehicle coordinates. Plausibility and consistency checks further validate its reliability for misbehaviour detection [10].

3) *Taxonomy of Attacks:* The dataset includes 19 attacks that span different traffic densities (high/low traffic density) and times of day (24 hours). The attack names, class labels assigned to each attack and their descriptions are detailed in

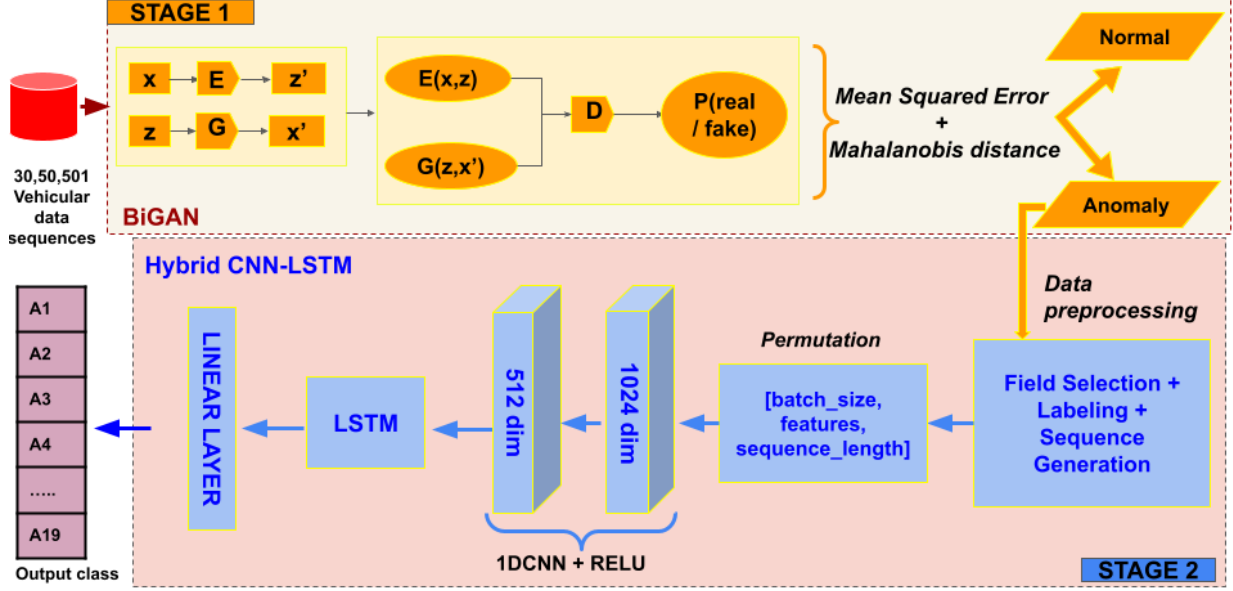


Fig. 2: Proposed FAST-IDS architecture.

[11].

IV. PROPOSED INTRUSION DETECTION FRAMEWORK

The proposed FAST-IDS architecture is illustrated in Fig. 2. The architecture consists of two stages. The first stage performs coarse-grained classification, distinguishing between normal and anomalous data, and the second stage conducts fine-grained classification, identifying the input sequence as one of 19 known attack types. We have further compressed this model to be deployed in resource-constrained environments.

A. Stage 1

1) *Data Preprocessing*: We have utilized the 24-hour benchmarked VeReMi Extension dataset [10], selecting the motion-related information in line with prior studies [11, 32, 33]. Each instance or sequence is denoted as Seq_i , where the i^{th} sequence includes features such as $(p_{x_i}, p_{y_i}, s_{x_i}, s_{y_i}, a_{x_i}, a_{y_i}, h_{x_i}, h_{y_i})$, corresponding to position, speed, acceleration, and heading in the x and y direction, respectively.

2) *Architectures Employed*: Each input sequence Seq_i is fed into the encoder E , a 5-layer CNN, which produces the latent code $E(x)$. This latent code is then fed into the generator G , a 4-layer CNN, which reconstructs the input sequence as Seq'_i . The discriminator D , also implemented as a 4-layer CNN, receives joint pairs from the encoder $(x, E(x))$ and the generator $(G(E(x)), E(x))$, and outputs a probability indicating whether the data originates from the encoder (real) or the generator (fake). The model is trained using the Wasserstein loss with a gradient penalty to enforce the Lipschitz constraint on discriminator weights.

where the value function $V(D, G, E)$ is given by

$$V(D, G, E) = \mathbb{E}_{x \sim p_{\text{data}}} [D(x, E(x))] - \mathbb{E}_{x \sim p_{\text{data}}} [D(G(E(x)), E(x))] + \lambda_{gp} \mathbb{E}_{\hat{x} \sim p_{\hat{x}}} \left[\left(\|\nabla_{\hat{x}} D(G(E(x)), E(x))\|_2 - 1 \right)^2 \right]. \quad (2)$$

Here, $\mathbb{E}_{x \sim p_{\text{data}}}$ refers to the expectation over data and λ_{gp} is the gradient penalty term.

3) *Sequence Reconstruction and Reconstruction Error Calculation*: The Seq'_i reconstructed by the generator corresponds to $(p'_{x_i}, p'_{y_i}, s'_{x_i}, s'_{y_i}, a'_{x_i}, a'_{y_i}, h'_{x_i}, h'_{y_i})$, representing the reconstructed values of position, speed, acceleration, and heading in the x and y directions, respectively. The Reconstruction Error (RE) was measured using weighted sum of Mean Squared Error (MSE) and Mahalanobis Distance (D_M) [34].

$$MSE = \frac{1}{n} \sum_{i=1}^n ((Seq_i) - (Seq'_i))^2 \quad (3)$$

$$D_M = \sqrt{(Seq'_i - \mu)^T \Sigma^{-1} (Seq'_i - \mu)} \quad (4)$$

Here, μ is the mean vector of the input data, Σ^{-1} is the inverse of the covariance matrix of the input data.

The combined score (RE) is calculated as follows:

$$\text{Combined Score} = \alpha \cdot D_M + (1 - \alpha) \cdot MSE \quad (5)$$

Here, $\alpha = 0.5$ is a weighting factor that balances the contributions of the Mahalanobis distance and the MSE. The Interquartile Range (IQR) was employed to determine the range of values within which the RE of the ground truth data lies.

$$\min_{G, E} \max_D V(D, G, E), \quad (1)$$

$$IQR = Q3 - Q1 \quad (6)$$

$$\text{Upper Limit (UL)} = Q3 + 1.5 \times \text{IQR} \quad (7)$$

$$\text{Lower Limit (LL)} = Q1 - 1.5 \times \text{IQR} \quad (8)$$

Q1 corresponds to the 25th percentile, whereas Q3 corresponds to the 75th percentile. We have utilized different quartiles to distinguish between anomalous and normal data.

$$\text{For ANOMALY} = \begin{cases} 1, & \text{for } RE < Q1 \text{ or } RE > Q3 \\ 0, & \text{otherwise} \end{cases} \quad (9)$$

$$\text{For NORMAL} = \begin{cases} 1, & \text{for } LL \leq RE \leq UL \\ 0, & \text{otherwise} \end{cases} \quad (10)$$

Here, LL and UL are linearly adjusted forms of Q1 and Q3, respectively.

B. Stage 2

1) *Data Preprocessing*: The data sequences [10] flagged as anomalous from Stage 1 are fed as input to Stage 2 [28]. To prepare the input data, we create fixed-length window sequences of size w , inspired by [2]. This approach produces sequences containing w consecutive samples, ensuring temporal order. Each sample Seq_{iA} is of the form $(p_{x_i}, p_{y_i}, s_{x_i}, s_{y_i}, a_{x_i}, a_{y_i}, h_{x_i}, h_{y_i})$, representing the features same as in Stage 1. As illustrated in Fig. 2, match the input expectations of the Hybrid CNN-LSTM model, the data is rearranged into the format *(batch_size, features, sequence_length)*.

2) *Architectures Employed and Multiclass Classification*: The input data Seq_{iA} is fed into a 2-layer CNN with ReLU activation to extract features. The generated latents are then passed into an LSTM, which captures temporal dependency. A dense head, represented by a single linear layer with softmax activation, maps these latents to class prediction probabilities. We have also experimented with the model using Bidirectional LSTM variant and various loss functions, including Cross-Entropy loss (CE), Label Smoothing Loss (SL), and Focal Loss (FL). The results are detailed in Section VI.

$$CE = -\frac{1}{N} \sum_{n=1}^N \sum_{i=1}^C y_i^n \log(p_i^n) \quad (11)$$

$$SL = -\frac{1}{N} \sum_{n=1}^N \sum_{i=1}^C \left((1 - \alpha) y_i^n + \frac{\alpha}{C} \right) \log(p_i^n) \quad (12)$$

$$FL = -\frac{1}{N} \sum_{n=1}^N \sum_{i=1}^C (1 - p_i^n)^\gamma y_i^n \log(p_i^n) \quad (13)$$

Here, N is the number of data points in the batch and C is the number of classes. y_i^n and p_i^n corresponds to the true and the predicted probability of the n -th data point for class i respectively. In Eq. 12, α is the smoothing parameter, which spreads probability across all classes and in Eq. 13 γ is the focus parameter that helps reduce the weights on the parameters.

C. Hybrid Model Compression

We implemented a two-stage model compression technique to enhance model efficiency. First, structured pruning was applied to convolutional layer filters using L1 importance with a pruning ratio, followed by fine-tuning for E epochs. Next, static quantization was performed on weights and activations using a min-max observer, with calibration conducted on a subset of the training dataset. We have utilized asymmetric quantization for activation and symmetric quantization for weights as suggested in prior studies [35]. The formula for structured pruning is as follows:

$$I_w = \sum |w^{pre}| \quad (14)$$

Here I_w is the importance score of filter, W^{pre} is the weights between the layers before compression. $|W^{pre}|$ gives the absolute value (L1 norm), after which we sort the filters in ascending order, discarding the least important weights based on pruning ratio p . After which, the model is fine-tuned for E epochs and then fed to the quantization module.

The static quantization formula for weights w and activations x are as follows:

$$\begin{aligned} w^q &= \text{clamp} \left(\text{round} \left(\frac{w^{\text{ft}}}{s} \right), -2^{n-1}, 2^{n-1} - 1 \right) \\ x^q &= \text{clamp} \left(\text{round} \left(\frac{x}{s} \right) + z, 0, 2^n - 1 \right) \end{aligned} \quad (15)$$

where, Scale Factor (s) and Zero-Point (z) are defined as follows:

$$s = \frac{w_{\max} - w_{\min}}{2^n - 1} \quad (16)$$

$$z = \text{round} \left(\frac{-w_{\min}}{s} \right) \quad (17)$$

Here s and z are used to calculate the quantized weights (w^q) and activations (x^q) corresponding to n bit width. The value of s and z depends on the weight tensors $[w_{\min}, w_{\max}]$ and on the activation tensors $[x_{\min}, x_{\max}]$, which are calculated during calibration. During inference, we dequantize the values utilizing the formula given below:

$$V_{\text{dequantized}} = s \times (V_{\text{quantized}} - z) \quad (18)$$

The Eq. 18 is applicable for both w^q and x^q , where $V_{\text{quantized}} = w^q$ or x^q . For symmetric quantization corresponding to weight tensors, z will be zero. The algorithm for the proposed FAST-IDS is outlined as follows in Algorithm 1 and Algorithm 2.

V. EXPERIMENTAL SETUP

This section provides details of the system specification, dataset specification, and model hyperparameters used in this study.

A. System Specification

The experiments were performed on an NVIDIA RTX A6000 GPU using a software environment that included

Algorithm 1 FAST-IDS Algorithm

```

1: Stage 1 of FAST-IDS ALG
2: Inputs:  $x$  = input data,  $z$  = noise vector
3: //  $E$  = Encoder,  $G$  = Generator,  $D$  = Discriminator
4: //  $\alpha$  = weighting factor
5: Output:  $\hat{y}$  = Final assigned class label.
6: for each training iteration do
7:   Sample real data  $x \sim p_{\text{data}}(x)$ 
8:   Encode real data:  $\hat{z} \leftarrow E(x)$ 
9:   Generate fake sample:  $\hat{x} \leftarrow G(\hat{z})$ 
10:  Train  $D$  on real pair  $(x, \hat{z})$  and fake pair  $(\hat{x}, \hat{z})$ 
11:  Update  $D$  by maximizing discriminator objective function (Eq. 2)
12:  Update  $E$  and  $G$  by minimizing generator and encoder objective function (Eq. 2)
13: end for

14: Compute Reconstruction Error (RE) as:
15:    $RE = \alpha \cdot D_m + (1 - \alpha) \cdot \text{MSE}$ , where:
16:    $\text{MSE}(x, \hat{x}) = \frac{1}{n} \sum_{i=1}^n (x_i - \hat{x}_i)^2$ 
17:    $D_m(x') = (x' - \mu)^T \Sigma^{-1} (x' - \mu)$ 

18: Compute percentiles:  $Q1 = 25^{\text{th}}$  percentile,  $Q3 = 75^{\text{th}}$  percentile
19: Compute IQR:  $\text{IQR} = Q3 - Q1$ 
20: Compute limits:
21:    $LL = Q1 - 1.5 \cdot \text{IQR}$  (Lower Limit)
22:    $UL = Q3 + 1.5 \cdot \text{IQR}$  (Upper Limit)

23: for each data point  $x$  do
24:   Compute anomaly score  $s$ 
25:   if  $s < Q1$  or  $s > Q3$  then
26:     Classify  $x$  as Anomalous  $\rightarrow D_a$ 
27:   end if
28:   if  $LL \leq s \leq UL$  then
29:     Classify  $x$  as Normal  $\rightarrow D_n$ 
30:   end if
31: end for

32: Stage 2 of FAST-IDS ALG
33: Input:  $D_a$  (data classified as anomalies from Stage 1)
34: //  $c$  = CNN feature maps,  $l$  = LSTM hidden representation,  $y_{\text{pred}}$  = class probabilities
35: for each batch of sequences from  $D_a$  do
36:    $c \leftarrow \text{ReLU}(\text{Conv1D}_2(\text{ReLU}(\text{Conv1D}_1(D_a))))$ 
37:    $l \leftarrow \text{LSTM}(c)$ 
38:    $y_{\text{pred}} \leftarrow \text{Softmax}(Wl + b)$ 
39:   Assign class label  $\hat{y} \leftarrow \arg \max(y_{\text{pred}})$ 
40: end for

```

Python 3.10.12, torch 2.1.1 and the VSCode IDE. The inference is carried out in NVIDIA RTX A6000, Jetson Nano (jetpack 4.6.6) and Google Colab CPU.

B. Dataset Specification

Table II presents the instances used for training and testing in Stage 1. The anomalous data from Stage 1 undergoes labelling per class and sequence generation with a window size of 20, which resulted in 57,000 sequences. The process resulted in the following number of sequences per class: A(1) - 3804, A(2) - 3793, A(3) - 3821, A(4) - 3701, A(5) - 3623, A(6) - 3886, A(7) - 3662, A(8) - 3705, A(9) - 3727, A(10) - 3776, A(11) - 3870, A(12) - 3745, A(13) - 12564, A(14) - 12103, A(15) - 12370, A(16) - 16981, A(17) - 3876, A(18) - 8122 and A(19) - 7654.

Algorithm 2 Hybrid Model Compression

```

1: Input:  $w^{\text{pre}}$  = weights before compression,  $\Theta$  = pre-trained full precision model
2: //  $p$  = prune factor (0.4),  $\mathcal{D}$  = calibration data,  $E$  = fine-tuning epochs (10)
3: //  $I_w$  = weight importance (L1 norm),  $s$  = scale factor,  $z$  = zero-point,  $n$  = no. of bits to quantize,  $w_{\text{min}}$ ,  $w_{\text{max}}$  = min / max values in weight tensor,  $x_{\text{min}}$  = minimum of the activation outputs
4: Output: Compressed model  $\Theta^q$  with quantized weights  $w^q$  and quantized activation  $x^q$ .
5: for each layer  $o_l$  in  $\Theta$  do
6:   Compute weight importance:  $I_w = \sum |w^{\text{pre}}|$ 
7:   Rank filters based on  $I_w$ 
8:   Prune least important  $p = 40\%$  filters  $\rightarrow w^{\text{pruned}}$ 
9: end for
10: Fine-tune the pruned model  $\Theta^*$  on  $\mathcal{D}$  for  $E = 10$  epochs to obtain  $w^{ft}$ 
11: Run calibration on  $\mathcal{D}$  to determine  $w_{\text{min}}$ ,  $w_{\text{max}}$  and  $x_{\text{min}}$ 
12: for each weight tensor  $w^{ft}$  in  $\Theta^*$  do
13:   Compute scale factor:  $s = \frac{w_{\text{max}} - w_{\text{min}}}{2^n - 1}$ 
14:   Compute zero-point:  $z = \text{round}(-\frac{w_{\text{min}}}{s})$ 
15:   Quantize weights (symmetric):
    
$$w^q = \text{clamp}\left(\text{round}\left(\frac{w^{ft}}{s}\right), -2^{n-1}, 2^{n-1} - 1\right)$$

16: end for
17: for each activation  $x$  do
18:   Quantize activations (asymmetric):
    
$$x^q = \text{clamp}\left(\text{round}\left(\frac{x}{s}\right) + z, 0, 2^n - 1\right)$$

19: end for
20: Save the final compressed quantized model  $\Theta^q$ ,  $s$  and  $z$  for dequantization.

```

TABLE II: Data Instances

S. No.	Instances	No. of Instances	Size
1	groundtruth / training	30,50,501	1.3 gb
2	normal / testing	1,18,78,433	6.1 gb
3	anomaly / testing	52,47,975	2.8 gb

C. Training and Testing

The training time for Stage 1 was 93,357.48 seconds, approximately 25.93 hours, whereas Stage 2 required 12,862.64 seconds, approximately 3.57 hours for modelling. In Stage 1, the model was trained for 30 epochs using the RMSProp optimizer with a learning rate of 0.0002. The gradient penalty lambda coefficient was set to 10, and the latent dimension was 100. In Stage 2, the model was trained for 100 epochs using the Adam optimizer with a learning rate of 0.0003.

VI. PERFORMANCE EVALUATION AND ANALYSIS OF RESULTS

This section provides numerical and graphical results of the proposed FAST-IDS network, demonstrating its effectiveness against various vehicular attacks. Additionally, the analysis includes comparisons with baseline SOTA methods, detection of previously unseen attacks, and the model's performance when deployed in a resource-constrained environment.

TABLE III: Recall values of Stage 1 models, highlighting the impact of architectural variations including number of layers utilized in encoder, decoder and generator and loss functions used on detection performance.

S. No.	Model used	Normal_recall	Anomaly_recall
1	BiGAN_WGAN_GP(5E_4G_4D)	0.9967	0.859
2	BiGAN_WGAN_GP(6E_4G_4D)	0.9998	0.5813
3	BiGAN_WGAN_GP(5E_5G_5D)	0.996	0.6595
4	BiGAN_WGAN_GP(4E_4G_4D)	0.9643	0.5331
5	BiGAN_WGAN(5E_4G_4D)	1	0.2565
6	BiGAN_BCE(5E_4G_4D)	0.8397	0.816
7	BiGAN_WGAN_GP(5E_4G_4D)_24h	0.95137	0.504612

A. Evaluation and Analysis for Stage 1

The models used in Stage 1 are as follows:

- BiGAN_WGAN_GP(5E_4G_4D) [M1] - BiGAN trained with Wasserstein's loss and Gradient Penalty, featuring a 5-layer CNN encoder, a 4-layer CNN generator, and a 4-layer CNN discriminator.
- BiGAN_WGAN_GP(6E_4G_4D) [M2] - BiGAN trained with Wasserstein's loss and Gradient Penalty, featuring a 6-layer CNN encoder, a 4-layer CNN generator, and a 4-layer CNN discriminator.
- BiGAN_WGAN_GP(5E_5G_5D) [M3] - BiGAN trained with Wasserstein's loss and Gradient Penalty, featuring a 5-layer CNN encoder, a 5-layer CNN generator, and a 5-layer CNN discriminator.
- BiGAN_WGAN_GP(4E_4G_4D) [M4] - BiGAN trained with Wasserstein's loss and Gradient Penalty, featuring a 4-layer CNN encoder, a 4-layer CNN generator, and a 4-layer CNN discriminator.
- BiGAN_WGAN(5E_4G_4D) [M5] - BiGAN trained with Wasserstein's loss without Gradient Penalty.
- BiGAN_BCE(5E_4G_4D) [M6] - BiGAN trained with Binary Cross Entropy.
- BiGAN_WGAN_GP(5E_4G_4D)_24h [M7] - BiGAN trained for 24 hours files individually.

The naming convention used for each of the models discussed above are closely related to the experiment configuration. Additionally, we have also included a short name such as M1 to M7, which is used as an annotation in Figures (Fig. 3). The recall values of Stage 1 models are illustrated in Table III, where Normal Recall represents the percentage of correctly identified normal instances, while Anomaly Recall indicates the percentage of correctly identified anomalous instances.

BiGAN_WGAN_GP(5E_4G_4D) achieves strong recall rates for normal and anomalous instances, benefiting from Wasserstein's loss with Gradient Penalty and its 5-layer CNN encoder architecture. In contrast, other variants such as BiGAN_WGAN_GP(6E_4G_4D) and BiGAN_WGAN_GP(5E_5G_5D) exhibit underfitting to anomalous data points, indicating that increasing the number of layers may negatively impact model performance. While BiGAN_WGAN_GP(4E_4G_4D) performs well on normal instances but struggles with anomalies, suggested that its 4-layer CNN encoder lacks the complexity of the 5-layer variant. BiGAN_WGAN(5E_4G_4D) achieves perfect recall for normal instances but overfits anomalies, reflecting the absence of

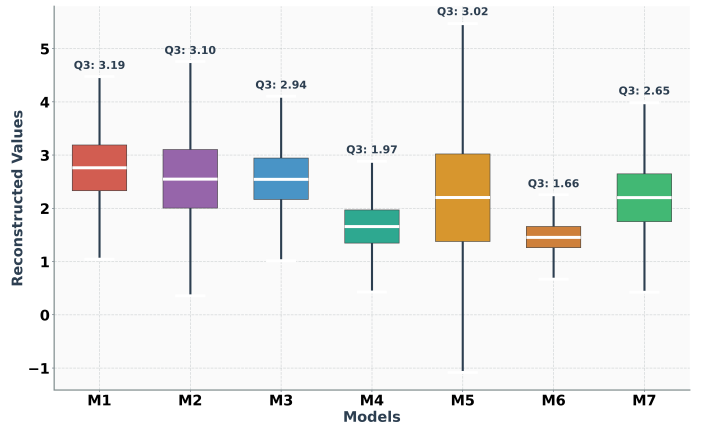


Fig. 3: Whisker boxplots of reconstruction error for the seven BiGAN model variants used in the ablation study in Stage 1. Each boxplot illustrates the IQR ranges between 1st quartile (Q1) and the 3rd quartile (Q3) and extends upto the Lower (LL) and Upper Limits (UL).

Gradient Penalty. BiGAN_BCE(5E_4G_4D) maintains strong performance across both instance types, benefiting from Binary Cross Entropy's reduced sensitivity to extreme values. Meanwhile, BiGAN_WGAN_GP(5E_4G_4D)_24h adapts to 24-hour data imbalance but underperforms on anomalies. Overall, BiGAN_WGAN_GP(5E_4G_4D) offers the best recall for both normal and anomalous instances, demonstrating robustness in anomaly detection, highlighting the importance of Gradient Penalty and complex CNN architectures in improving anomaly detection.

To further analyze the BiGAN variants' behaviour, we plotted the whisker boxplot in Fig. 3. The distributions are based on IQR ranges, highlighting the variability of each model's reconstruction error. The BiGAN_WGAN(5E_4G_4D) [M5] variant with broader reconstruction error, showcase poor performance, while model BiGAN_WGAN_GP(5E_4G_4D) [M1], with tighter distributions and compact IQR, illustrate superiority in input reconstruction and anomaly detection. But as the plot becomes more narrower, the the model also struggles to detect anomaly (BiGAN_WGAN_GP(4E_4G_4D) [M4]) and normal data (BiGAN_BCE(5E_4G_4D) [M6]).

B. Evaluation and Analysis for Stage 2

The models used in Stage 2 are as follows:

- CNN_LSTM_CE - The hybrid model, consisting of 1 CNN and 1 LSTM, was updated using cross-entropy loss.
- 2CNN_LSTM_CE - The hybrid model, consisting of 2 CNN and 1 LSTM, was updated using cross-entropy loss.
- 2CNN_BiLSTM_CE - The hybrid model, consisting of 2 CNN and 1 Bidirectional LSTM, was updated using cross-entropy loss.
- 2CNN_LSTM_LSmooth - The hybrid model, consisting of 2 CNN and 1 LSTM, was updated using label smoothing Loss.
- 2CNN_LSTM_FL - The hybrid model, consisting of 2 CNN and 1 LSTM, was updated using focal loss.

TABLE IV: Overall Performance Metrics Across Stage 2 Models, highlighting the impact of number of layers and loss function in the hybrid CNN-LSTM model.

Model	Acc	Precision	Recall	F1-score
CNN_LSTM_CE	97.81	78.55	78.07	78.05
2CNN_LSTM_CE	97.80	78.75	78.01	78.17
2CNN_BiLSTM_CE	97.81	78.55	78.07	78.05
2CNN_LSTM_LSmooth	97.88	79.42	78.81	78.21
2CNN_LSTM_FL	97.81	78.72	78.14	78.15

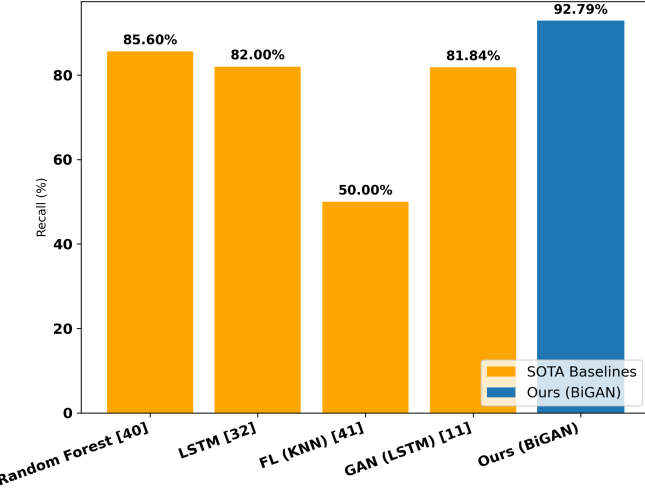


Fig. 4: Graph illustrating the performance of FAST-IDS (Stage 1) with respect to other SOTA baselines in terms of recall percentages.

The results presented in Tables IV illustrate the performance metrics for Stage 2 models.

The choice of hybrid CNN-LSTM models is justified by their strong performance, as evidenced in [2], [38] and [39]. Among the models presented in Table IV, CNN_LSTM_CE underperforms in performance compared to other models, while 2CNN_LSTM_CE achieves the better accuracy and balanced performance due to an additional CNN layer capturing more complex features. The bidirectional variant (2CNN_BiLSTM_CE) performs similarly to 2CNN_LSTM_CE, showing minimal improvement over 2CNN_LSTM_CE in accuracy and recall. 2CNN_LSTM_LSmooth demonstrates comparatively the best performance, indicating that label smoothing loss effectively balances these metrics and slightly outperforms the focal loss model (2CNN_LSTM_FL). The results emphasize the role of model architecture and loss functions in multiclass classification, with 2CNN_LSTM_LSmooth delivering balanced performance. Since 2CNN_LSTM_LSmooth yielded the best results, we experimented with increasing the layers of CNN and LSTM for this variant. While this maintained performance similar to 2CNN_LSTM_LSmooth, it resulted in a significant increase in computational time. The confusion matrix presented in Fig. 5 provides a detailed view of the classification performed by the 2CNN_LSTM_LSmooth model, demonstrating the correctly and the wrongly classified samples per class.

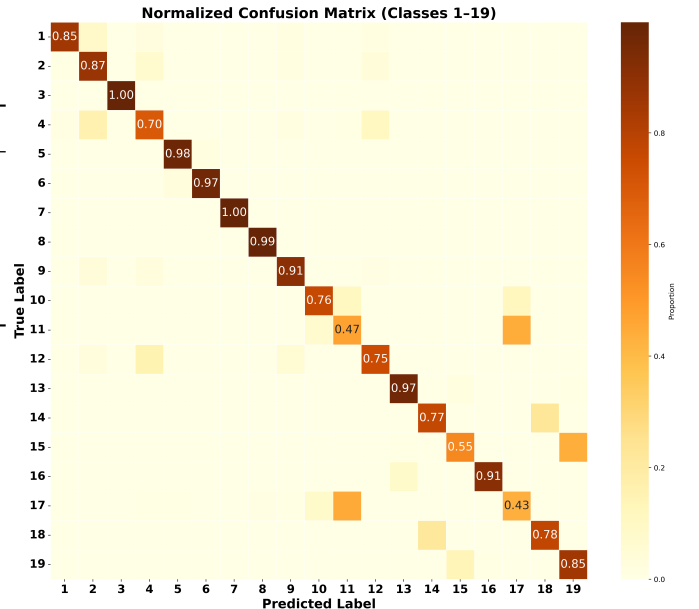
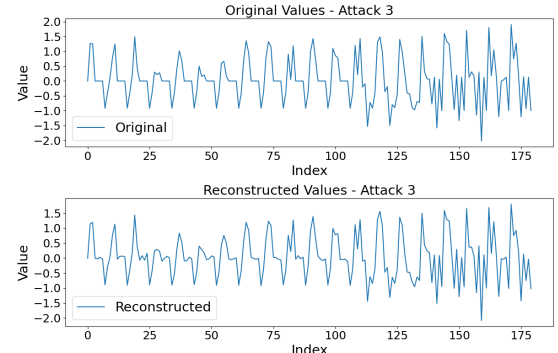
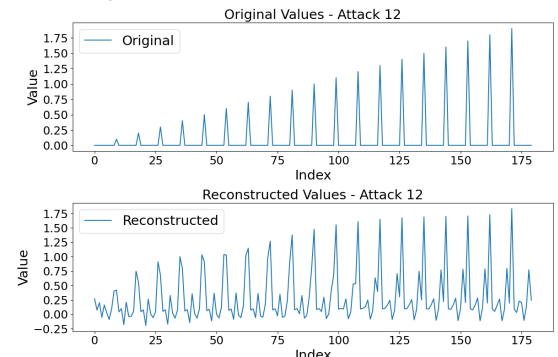


Fig. 5: The confusion matrix visualized as the heat map of the Stage 2 Hybrid CNN-LSTM model evaluated across 19 attack classes.



(a) Original and Reconstructed Plots for Attack 3.



(b) Original and Reconstructed Plots for Attack 12.

Fig. 6: Comparison of Original and Reconstructed Plots

Our study observed that only limited studies have performed multi-stage intrusion detection in CAVs utilizing the VeReMi extension dataset [10]. For Stage 1, we have compared our work with existing methodologies implementing binary classification [32, 40, 41] or anomaly detection systems [11]. In contrast, for Stage 2, we benchmarked against studies that

TABLE V: Summarized results illustrating the effectiveness of our Two-Stage Intrusion Detection Framework.

Stage	Model	Accuracy (%)	Precision (%)	Recall (%)	F1-score (%)
Stage 1	BiGAN_WGAN_GP(5E_4G_4D)	95.44	100	92.79	96.12
Stage 2	2CNN_LSTM_LSmooth	97.88	79.42	78.81	78.21

TABLE VI: Comparison of Recall Rates for Various Attack Classes with SOTA for Stage 2

Attack Class	Our Model	[28]	[36]	[33]	[37]
A(1)	82.50	42.5	82.34	54.12	65
A(2)	78.33	5.5	74.67	99.96	69
A(3)	100	100	99.30	99.82	61
A(4)	60.83	8	99.36	99.20	71
A(5)	97.83	94.5	81.81	99.88	59
A(6)	97.17	42	3.81	100	61
A(7)	100	100	99.48	98.73	49
A(8)	100	100	98.55	100	61
A(9)	85.83	9	6.53	99.70	71
A(10)	79.17	98.5	6.81	99.73	58
A(11)	53.83	98.5	99.92	78.12	62
A(12)	65.17	8.5	99.90	99.97	56
A(13)	96.17	98	78.25	94.91	56
A(14)	78.67	100	78.88	99.98	50
A(15)	56.83	99.5	60.04	99.93	56
A(16)	98.50	98.5	2.78	100	62
A(17)	43.17	97.5	53.26	100	58
A(18)	91.83	100	79.58	88.23	62
A(19)	86.83	99	76.93	99.67	63

focused on multi-class classification [28, 33, 36, 37].

The results corresponding to the best performing models in Stage 1 and 2 are presented in Table V.

C. Stage 1 Comparison with SOTA

An extensive comparison with baseline models [11, 32, 40, 41] are illustrated in Fig. 4. Our model demonstrates superior overall performance compared to the SOTA, with a recall percentage of 92.785%. Compared to Random Forest utilized in [40], LSTM in [32], Federated Learning with KNN utilized in [41], and GAN with LSTM utilized in [11], our model achieved a relative improvement of 30.25%, clearly demonstrating the superiority of FAST-IDS in detecting anomalous behaviour. This relative improvement is due to the integration of BiGAN with WGAN features, which stabilized training of the model. Unlike traditional models such as KNN and Random Forest, which provided limited representation learning and standard GAN prone to model collapse, our model succeeded in capturing both temporal and spatial structures in the data.

D. Stage 2 Comparison with SOTA

Stage 2 is evaluated against single-stage classifiers [28, 33, 36, 37] to demonstrate the effectiveness of our multi-stage model and the comparisons are illustrated in Table VI. Our results are comparable in 11 attack types in both [28] and [36] individually - Constant position (A1), Constant

position offset (A2), Random position (A3), Random position offset (A4), Constant speed (A5), Constant speed offset (A6), Random speed (A7), Random speed offset (A8), Eventual Stop (A9), Delayed messages (A12) and Data replay Sybil (A16) [28]. While [28] employed a CNN, we utilized Hybrid CNN-LSTM models. This difference might explain why [28] yielded very low recall values for Constant position offset (A2), Random position offset (A4), Eventual Stop (A9), and Delayed messages (A12). On the other hand, [33] developed an integrated approach combining CNN, LSTM and Support Vector Machine (SVM) and demonstrated exceptional results, but it lacks generalization capability. In comparison with [37] which uses a tree-based classifier, our model demonstrates a clear advantage in outperforming in 16 attacks.

E. Detection of Previously Unseen Attacks

Stage 1 employs BiGAN for detecting unseen data through its reconstructive properties. In Stage 2, the dataset was split into known (A0–A9) and unknown (A10–A19) attacks. The model was trained and validated on known attacks and tested on known and unknown attacks. A reconstructive layer was added after LSTM, enabling the model to learn input patterns effectively. The Mean Squared Error (MSE) between the input and the reconstructed data was used as the reconstruction error. We have employed a percentile-based thresholding strategy to address the dynamic and evolving nature of attacks. Here, the 91st percentile of the reconstruction errors from the validation set was selected as the decision boundary. Various threshold ranges between 80 and 93 were evaluated, while 91 yielded the best tradeoff between known and unknown classes. The accuracies within unseen data are as follows: Class 10: 97.83%, Class 11: 82.33%, Class 12: 50.17%, Class 13: 54.67%, Class 14: 100.00%, Class 15: 100.00%, Class 16: 81.17%, Class 17: 84.50%, Class 18: 100.00%, and Class 19: 99.83%. As shown in Fig. 6a and 6b, the reconstructed plot for A(3) (known attack) closely matches the original, confirming accurate reconstruction, whereas A(12) (unknown attack) deviates significantly, validating its classification as an anomaly.

F. Computational Efficiency

To enhance efficiency and manage computational demands, we evaluated the model using hybrid data compression techniques, incorporating L1-based structured pruning followed by static quantization. We achieved a 54.4% reduction in model size through pruning and 77.2% reduction through quantization, leading to 34.17% reduction in FLOPs and a 54.15% reduction in MACs, thereby significantly enhancing computational efficiency. This optimization resulted in approximately 50.05% reduction in inference time with 5%

TABLE VII: Evaluation of Model Compression Techniques Across Different Environments

Environment	Inference Time (s)	M/y Utilization (MiB)	Compression Statistics				
			Model (%)	Reduction	Performance (%)	Loss	Reduced FLOPs / MMACs (%)
RTX A6000 GPU	2.2765	3428.21					
Google Colab CPU	7.938	1636.52	77.2		5		34.17 / 54.15
Jetson Nano	102.62	3353.34					

performance loss, as presented in Table VII, demonstrating significant computational efficiency improvements. Our model achieved attack detection within 0.195 seconds (per vehicle) on Jetson Nano, highlighting its efficiency for real-time deployment in resource-constrained environments. As part of the ablation study, we also evaluated random filter pruning, achieving 47.36% model compression but with a 16% performance loss. Additionally, L1 unstructural pruning led to a 40.59% model size reduction but achieved only 1.5x faster inference, highlighting the effectiveness of our proposed hybrid approach.

G. Comparison of Run Time Results with SOTA

The inference time for data setup and prediction is critical for real-time IDS performance. During inference, 10,000 sequences corresponding to 526 vehicles were considered. As shown in Table VIII, our compressed model achieves faster inference than [28] utilizing a reconstruction-based CNN model, [9] using a 4-layer LSTM, and [39] using a hybrid CNN-BiLSTM, significantly improving computational efficiency. This enhancement makes the model well-suited for real-time intrusion detection in autonomous vehicles, enabling fast threat identification and response in dynamic vehicular networks.

TABLE VIII: Inference Time Comparison on Jetson Nano with SOTA

Reference	Environment	Data Setup	Prediction	Inference Time (ms)
[28]		0.07	511.82	511.89
[9]	Jetson Nano	287.74	0.33	288.07
[39]		370.92	0.395	371.32
Ours		0.003	194.997	195

VII. CONCLUSION

This paper presents a two-stage intrusion detection framework for Connected and Autonomous Vehicles (CAVs), optimized through hybrid model compression for enhanced computational efficiency and real-time deployment. The compression technique combines structural pruning using the L1 norm and static quantization, utilizing a min-max observer for calibration. This reduces model size by 77.2% and achieves approximately 50.05% reduction in inference time, enabling per-vehicle attack detection on Jetson Nano in 0.195 ms, making it suitable for resource-constrained Intelligent Transportation Systems (ITS). The proposed two-stage architecture combines a Bidirectional Generative Adversarial Network (BiGAN) with

Wasserstein loss, gradient penalty, and a deep CNN architecture leveraging reconstruction error using Mean Squared Error (MSE) and Mahalanobis distance, with a hybrid CNN-LSTM in Stage 2 trained with label smoothing loss. Together, both stages enable the detection of previously unseen attacks. At the same time, hybrid model compression ensures efficient, accurate, and real-time attack detection in CAV networks, making it highly adaptable for real-world ITS applications. Our two-stage model explicitly addresses the uncertainties in IDS, such as previously unseen attack types, changing traffic scenarios, and unpredictable behaviour of attackers, through the BiGAN anomaly detector and the Hybrid CNN-LSTM intrusion detector. Although the hybrid compression technique may introduce additional uncertainties, our framework achieved comparable detection rates and faster inference over baseline models.

Future work will focus on developing more lightweight architectures, advancing model compression techniques, and exploring Federated Learning for decentralized training to enhance data privacy and reduce communication overhead in large-scale vehicular networks. Also, we plan to explore adaptive feature elimination and redundancy-aware mechanisms to deal with computational efficiency, and an online thresholding mechanism to deal with anomaly detection.

REFERENCES

- [1] S. Kumari, H. Xiong, L. Khoukhi, and J. J. Rodrigues, “Safety and security of autonomous vehicles,” p. e4880, 2023.
- [2] T. Alladi, V. Kohli, V. Chamola, F. R. Yu, and M. Guizani, “Artificial intelligence (ai)-empowered intrusion detection architecture for the internet of vehicles,” *IEEE Wireless Communications*, vol. 28, no. 3, pp. 144–149, 2021.
- [3] A. Festag, “Cooperative intelligent transport systems standards in europe,” *IEEE Communications Magazine*, vol. 52, no. 12, pp. 166–172, 2014.
- [4] S. E. Shladover, “Connected and automated vehicle systems: Introduction and overview,” *Journal of Intelligent Transportation Systems*, vol. 22, no. 3, pp. 190–200, 2018.
- [5] S. Kumar, S. Velliangiri, P. Karthikeyan, S. Kumari, S. Kumar, and M. K. Khan, “A survey on the blockchain techniques for the internet of vehicles security,” *Transactions on Emerging Telecommunications Technologies*, vol. 35, no. 4, p. e4317, 2024.
- [6] J. Xiao, Y. Ren, J. Du, Y. Zhao, S. Kumari, M. J. Alenazi, and H. Yu, “Calra: practical conditional anonymous and leakage-resilient authentication scheme for vehicular crowdsensing communication,” *IEEE Transactions on Intelligent Transportation Systems*, 2024.
- [7] M. Ismail, S. Chatterjee, J. K. Sing, S. Kumari, and J. J. Rodrigues, “Designing anonymous key agreement scheme for secure vehicular ad-hoc networks,” *IEEE Transactions on Intelligent Transportation Systems*, 2024.
- [8] M. A. Akram, A. N. Mian, and S. Kumari, “Fog-based low latency and lightweight authentication protocol for vehicular communication,” *Peer-to-Peer Networking and Applications*, vol. 16, no. 2, pp. 629–643, 2023.

[9] T. Alladi, V. Kohli, V. Chamola, and F. R. Yu, "A deep learning based misbehavior classification scheme for intrusion detection in cooperative intelligent transportation systems," *Digital Communications and Networks*, vol. 9, no. 5, pp. 1113–1122, 2023.

[10] J. Kamel, M. Wolf, R. W. Van Der Hei, A. Kaiser, P. Urien, and F. Kargl, "Veremi extension: A dataset for comparable evaluation of misbehavior detection in vanets," in *Proceedings of the ICC 2020-2020 IEEE International Conference on Communications (ICC)*, 2020, pp. 1–6.

[11] D. S. R. R. Shrivastava, P. Narang, T. Alladi, and F. R. Yu, "Vadgan: An unsupervised gan framework for enhanced anomaly detection in connected and autonomous vehicles," *IEEE Transactions on Vehicular Technology*, vol. 73, no. 9, pp. 12 458–12 467, 2024.

[12] M. Sreelekshmi and S. Aji, "A deep architecture for in-vehicle intrusion detection using controller area network-graph relied feature images," *Computers and Electrical Engineering*, vol. 127, p. 110584, 2025.

[13] M. Sajid, K. R. Malik, A. Almogren, T. S. Malik, A. H. Khan, J. Tanveer, and A. U. Rehman, "Enhancing intrusion detection: a hybrid machine and deep learning approach," *Journal of Cloud Computing*, vol. 13, no. 1, p. 123, 2024.

[14] D.-h. Lee, D.-y. Kim, and J.-i. Jung, "Multi-stage intrusion detection system using hidden markov model algorithm," in *Proceedings of the International Conference on Information Science and Security (ICISS 2008)*, 2008, pp. 72–77.

[15] P. Zhou, G. Zhou, D. Wu, and M. Fei, "Detecting multi-stage attacks using sequence-to-sequence model," *Computers & Security*, vol. 105, p. 102203, 2021.

[16] C.-M. Chen, Z. Li, S. Kumari, G. Srivastava, K. Lakshmann, and T. R. Gadekallu, "A provably secure key transfer protocol for the fog-enabled social internet of vehicles based on a confidential computing environment," *Vehicular Communications*, vol. 39, p. 100567, 2023.

[17] W. Kim, J. Lee, Y. Lee, Y. Kim, J. Chung, and S. Woo, "Vehicular multilevel data arrangement-based intrusion detection system for in-vehicle can," *Security and Communication Networks*, vol. 2022, no. 1, p. 4322148, 2022.

[18] Y.-R. Lee, N.-E. Park, S.-Y. Kim, and I.-G. Lee, "Malicious traffic compression and classification technique for secure internet of things," *Computers, Materials and Continua*, vol. 76, no. 3, pp. 3465–3482, 2023.

[19] M. Althunayyan, A. Javed, and O. Rana, "A robust multi-stage intrusion detection system for in-vehicle network security using hierarchical federated learning," *Vehicular Communications*, vol. 49, p. 100837, 2024.

[20] G. Xie, L. T. Yang, Y. Yang, H. Luo, R. Li, and M. Alazab, "Threat analysis for automotive can networks: A gan model-based intrusion detection technique," *IEEE Transactions on Intelligent Transportation Systems*, vol. 22, no. 7, pp. 4467–4477, 2021.

[21] Q. Zhao, M. Chen, Z. Gu, S. Luan, H. Zeng, and S. Chakraborty, "Can bus intrusion detection based on auxiliary classifier gan and out-of-distribution detection," *ACM Transactions on Embedded Computing Systems (TECS)*, vol. 21, no. 4, pp. 1–30, 2022.

[22] J. Donahue, P. Krähenbühl, and T. Darrell, "Adversarial feature learning," *arXiv preprint arXiv:1605.09782*, 2016.

[23] M. A. Amanullah, M. B. Chhetri, S. W. Loke, and R. Doss, "Burst-adma: Towards an australian dataset for misbehaviour detection in the internet of vehicles," in *Proceedings of the IEEE International Conference on Pervasive Computing and Communications Workshops and other Affiliated Events (PerCom Workshops)*, 2022, pp. 624–629.

[24] C. Fan, J. Cui, H. Jin, H. Zhong, I. Bolodurina, and D. He, "Auto-updating intrusion detection system for vehicular network: A deep learning approach based on cloud-edge-vehicle collaboration," *IEEE Transactions on Vehicular Technology*, vol. 73, no. 10, pp. 15 372–15 384, 2024.

[25] P. Sharma and H. Liu, "A machine-learning-based data-centric misbehavior detection model for internet of vehicles," *IEEE Internet of Things Journal*, vol. 8, no. 6, pp. 4991–4999, 2020.

[26] P. Sharma, D. Austin, and H. Liu, "Attacks on machine learning: Adversarial examples in connected and autonomous vehicles," in *Proceedings of the IEEE International Symposium on Technologies for Homeland Security (HST)*, 2019, pp. 1–7.

[27] S. Ullah, M. A. Khan, J. Ahmad, S. S. Jamal, Z. e Huma, M. T. Hassan, N. Pitropakis, Arshad, and W. J. Buchanan, "Hdl-ids: a hybrid deep learning architecture for intrusion detection in the internet of vehicles," *Sensors*, vol. 22, no. 4, p. 1340, 2022.

[28] A. Chougule, V. Kohli, V. Chamola, and F. R. Yu, "Multibranch reconstruction error (mbre) intrusion detection architecture for intelligent edge-based policing in vehicular ad-hoc networks," *IEEE Transactions on Intelligent Transportation Systems*, vol. 24, no. 11, pp. 13 068–13 077, 2022.

[29] O. Tutsoy and H. E. Sumbul, "A novel deep machine learning algorithm with dimensionality and size reduction approaches for feature elimination: thyroid cancer diagnoses with randomly missing data," *Briefings in Bioinformatics*, vol. 25, no. 4, p. bbae344, 2024.

[30] R. W. Van Der Heijden, T. Lukaseder, and F. Kargl, "Veremi: A dataset for comparable evaluation of misbehavior detection in vanets," in *Security and Privacy in Communication Networks: 14th International Conference, SecureComm 2018, Singapore, Singapore, August 8–10, 2018, Proceedings, Part I*. Springer, 2018, pp. 318–337.

[31] C. Sommer, D. Eckhoff, A. Brummer, D. S. Buse, F. Hagenauer, S. Joerer, and M. Segata, "Veins: The open source vehicular network simulation framework," *Recent advances in network simulation: the OMNeT++ environment and its ecosystem*, pp. 215–252, 2019.

[32] N. C. Kushardianto, S. Ribouh, Y. El Hillali, and C. Tatkeu, "Vehicular network anomaly detection based on 2-step deep learning framework," *Vehicular Communications*, vol. 49, p. 100802, 2024.

[33] H.-Y. Hsu, N.-H. Cheng, and C.-W. Tsai, "A deep learning-based integrated algorithm for misbehavior detection system in vanets," in *Proceedings of the 2021 ACM International Conference on Intelligent Computing and its Emerging Applications*, 2021, pp. 53–58.

[34] Y. Xu, Z. Wu, J. Chanusot, and Z. Wei, "Joint reconstruction and anomaly detection from compressive hyperspectral images using mahalanobis distance-regularized tensor rpca," *IEEE Transactions on Geoscience and Remote Sensing*, vol. 56, no. 5, pp. 2919–2930, 2018.

[35] M. Nagel, M. Fournarakis, R. A. Amjad, Y. Bondarenko, M. Van Baalen, and T. Blankevoort, "A white paper on neural network quantization," *arXiv preprint arXiv:2106.08295*, 2021.

[36] O. Slama, B. Alaya, S. Zidi, and M. Tarhouni, "Comparative study of misbehavior detection system for classifying misbehaviors on vanet," in *2022 8th International Conference on Control, Decision and Information Technologies (CoDIT)*, vol. 1. IEEE, 2022, pp. 243–248.

[37] O. Slama, M. Tarhouni, S. Zidi, and B. Alaya, "One versus all binary tree method to classify misbehaviors in imbalanced veremi dataset," *IEEE Access*, vol. 11, pp. 135 944–135 958, 2023.

[38] A. Chougule, I. Kulkarni, T. Alladi, V. Chamola, and F. R. Yu, "Hybridsecnet: In-vehicle security on controller area networks through a hybrid two-step lstm-cnn model," *IEEE Transactions on Vehicular Technology*, vol. 73, no. 10, pp. 14 580–14 591, 2024.

[39] T. Alladi, B. Gera, A. Agrawal, V. Chamola, and F. R. Yu, "Deepadv: A deep neural network framework for anomaly detection in vanets," *IEEE Transactions on Vehicular Technology*, vol. 70, no. 11, pp. 12 013–12 023, 2021.

[40] R. Drenyovszki and Z. C. Johanyák, "Development of an attack detection module for vehicular ad-hoc networks," in *2024 IEEE 18th International Symposium on Applied Computational Intelligence and Informatics (SACI)*. IEEE, 2024, pp. 000 255–000 260.

[41] T. Moulahi, R. Jabbar, A. Alabdulatif, S. Abbas, S. El Khediri, S. Zidi, and M. Rizwan, "Privacy-preserving federated learning cyber-threat detection for intelligent transport systems with blockchain-based security," *Expert Systems*, vol. 40, no. 5, p. e13103, 2023.